Analysis Tools for Assessing the Impact of Wind Power on Weak Grids

Sina Sadeghi Baghsorkhi, *Student Member, IEEE* Ian A. Hiskens, *Fellow, IEEE*

***Abstract*—The integration of inherently variable wind generation into weak grids, particularly sub-transmission networks that are characterized by low X/R ratios, affects bus voltages, regulating devices and line flows. The meshed structure of these networks adds to the complexity, especially when wind generation is distributed across multiple nodes. This paper considers a range of techniques for analyzing the impact of wind variability on weak grids. Sensitivity analysis, based on the power-flow Jacobian, is used to highlight the sections of the system that are most severely affected by wind-power variations. A continuation power flow is used to determine parameter changes that reduce the impact of wind-power variability. It is also used to explore interactions between multiple wind-farms. Two optimization problems have been formulated to identify line segments that are most vulnerable to congestion as wind-power varies. The DC optimization is computationally more efficient, whereas the AC sensitivity-based optimization provides greater accuracy.**

***Index Terms*—Wind generation; sensitivity analysis; continuation methods; quadratic optimization; voltage regulation; line congestion.**

I. Introduction

WIND generation introduces high variability into sub-transmission networks (40-120 kV), significantly influencing the statistical characteristics of voltages and power flows. Wind power also often leads to bi-directional flows in distribution networks that were designed for uni-directional operation. Interconnections within sub-transmission networks further complicate power flow patterns induced by wind generation, particularly when wind-farms are distributed across multiple nodes of the network.

The variability inherent in the power produced by distributed wind-farms can lead to reactive power requirements that may adversely affect bus voltages and transformer tapping. In particular, legacy voltage regulation schemes may be ill-equipped to cope with the variations in power flow induced by wind generation. Wind-farm operators are required to regulate the voltage at their point-of-interconnection. However that requirement does not ensure voltages throughout the network are well-behaved. In fact, if voltage controls are not carefully coordinated, voltage regulating transformers may undergo excessive tapping, leading to a significant increase in maintenance. Furthermore, wind-power generation at multiple nodes can create unanticipated power flow patterns within the sub-transmission network. This may result in line congestion at power production levels that are far below the rated capacity of the wind-farms.

The effects of wind generation on the grid are often not obvious *a priori*. Standard power flow simulations provide limited insights, with few systematic methods available for analyzing the impact of wind on network voltages, tap-changer operation and line flows. This paper considers a range of analysis tools for assessing the impact of wind generation, and in particular evaluating voltage regulation and line congestion. These tools have been used to study a region of the Michigan power system where significant growth in wind generation is expected. It is anticipated that this increased wind generation will cause operational difficulties, including voltage variability and line overloading. These issues have been explored further in [1].

The paper is organized as follows. Sensitivity analysis is presented in Section II and continuation power flows are considered in Section III. An optimization formulation for assessing line congestion is developed in Section IV. Conclusions are presented in Section V.

II. Sensitivity Analysis

The power flow is fundamental to power system analysis, underpinning studies from contingency analysis to system planning. The power flow problem consists of a set of nonlinear algebraic equations that can be expressed as,

$$P(\theta, V) = 0 \tag{1}$$

$$Q(\theta, V) = 0 \tag{2}$$

where (1) describes the active power balance at PV and PQ buses, (2) describes the reactive power balance at PQ buses, θ is the vector of voltage angles (relative to the slack bus) at all PV and PQ buses, and V is the vector of voltage magnitudes at PQ buses [2]. It follows that P and θ have the same dimensions, and likewise the dimensions of Q and V are equal.

Transformer taps can be incorporated into the power flow equations by assuming tap positions a_i are continuous variables, and noting that each transformer regulates a particular bus voltage. That bus voltage magnitude V_i takes on a known fixed value, and so it can be replaced in (1)-(2) by the new variable a_i. The power flow equations can be generalized accordingly by replacing the voltage vector V with $\mathcal{V} = \begin{bmatrix} \tilde{V} \\ a \end{bmatrix}$ where $\tilde{V}$ is the vector of voltage magnitudes at non-regulated buses, and a is the vector of tap positions associated with the

Research supported by the Department of Energy through grant DE-EE0001382.

Sina Sadeghi Baghsorkhi (sinasb@umich.edu) and Ian A. Hiskens (hiskens@umich.edu) are with the Department of Electrical Engineering and Computer Science, University of Michigan, Ann Arbor, Michigan.

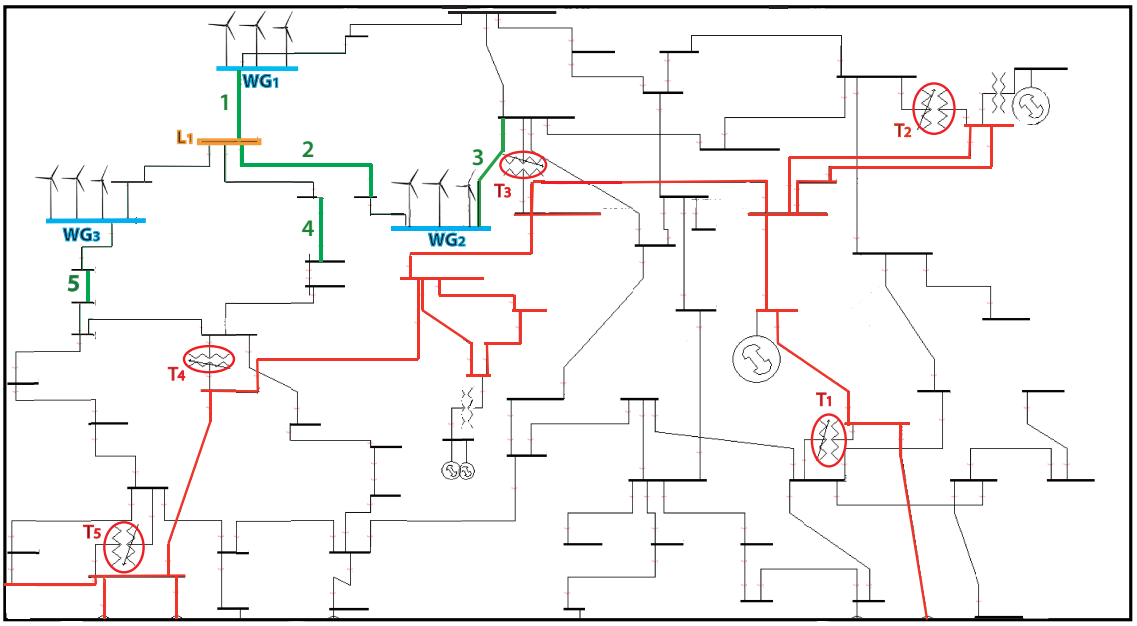

Fig. 1. Wind development network: wind injection nodes (blue), load bus L_1 (yellow), the 120 kV transmission system and the 120/40 kV tap-changing transformers (red), the 40 kV sub-transmission network (black). Lines of interest in the later congestion study are shown in green.

transformers that are regulating bus voltages. Note that Q and $\mathcal{V}$ still have equal dimensions.

Taking partial derivatives of P and Q with respect to θ and $\mathcal{V}$ gives the linearized relationship,

$$\begin{bmatrix}\Delta P\\ \Delta Q\end{bmatrix} = \begin{bmatrix}P_\theta & P_\mathcal{V}\\ Q_\theta & Q_\mathcal{V}\end{bmatrix}\begin{bmatrix}\Delta\theta\\ \Delta\mathcal{V}\end{bmatrix} \tag{3}$$

where $P_\theta \equiv \frac{\partial P}{\partial \theta}$, and likewise for the other sub-matrices. We are interested in how variations ΔP in the injected active power at wind-farm locations affect voltage magnitudes and tap positions, which are given by $\Delta\mathcal{V} = \begin{bmatrix}\Delta\tilde{V}\\ \Delta a\end{bmatrix}$. For transmission systems, where resistance is negligible, the off-diagonal blocks in (3) are almost zero, and so are normally neglected. This decouples ΔP from $\Delta\mathcal{V}$. However in sub-transmission and distribution networks, where resistance is non-negligible, the off-diagonal blocks become important. To understand how $\Delta\mathcal{V}$ varies with ΔP, we can use the Matrix Inversion Lemma [3] to give,

$$\begin{aligned}\Delta\mathcal{V} = &-\left[Q_\mathcal{V} - Q_\theta P_\theta^{-1} P_\mathcal{V}\right]^{-1} Q_\theta P_\theta^{-1}\Delta P\\ &+\left[Q_\mathcal{V} - Q_\theta P_\theta^{-1} P_\mathcal{V}\right]^{-1}\Delta Q.\end{aligned} \tag{4}$$

In our analysis, we assume that reactive power remains unchanged at PQ buses, so $\Delta Q = 0$. It follows that the desired sensitivities are given by,

$$\begin{aligned}\Delta\mathcal{V} &= -\left[Q_\mathcal{V} - Q_\theta P_\theta^{-1} P_\mathcal{V}\right]^{-1} Q_\theta P_\theta^{-1}\Delta P\\ &= S_\mathcal{V}\,\Delta P\end{aligned} \tag{5}$$

TABLE I
TAP STEP SENSITIVITIES FOR THE TRANSFORMERS HIGHLIGHTED IN FIGURE 1.

Transformer Tap-Ratio Sensitivities ($\frac{\text{tap-ratio}}{\text{MW injection}}$)						
Operating Point	Inject. Node	Transformer				
		T_1	T_2	T_3	T_4	T_5
Low wind injection	WG_1	0.04	0.04	0.10	0.11	0.07
	WG_2	0.05	0.04	0.14	0.09	0.06
Medium wind injection	WG_1	0.04	0.04	0.09	0.05	0.05
	WG_2	0.08	0.07	0.20	0.18	0.14
High wind injection	WG_1	0.03	0.01	0.02	0.03	0.05
	WG_2	0.03	0.01	0.02	0.03	0.06

where $S_\mathcal{V} = \begin{bmatrix}S_{\tilde{V}}\\ S_a\end{bmatrix}$, and

$\Delta\tilde{V} = S_{\tilde{V}}\Delta P$ for buses where voltages are not regulated,
$\Delta a = S_a \Delta P$ for transformer taps.

In later analysis, we will also make use of,

$$\begin{aligned}\Delta\theta &= \left[P_\theta - P_\mathcal{V} Q_\mathcal{V}^{-1} Q_\theta\right]^{-1}\Delta P\\ &= S_\theta\,\Delta P.\end{aligned} \tag{6}$$

Table I lists the sensitivity values of transformer tap-ratio to wind injection at WG_1 and WG_2 in the 40 kV sub-transmission network shown in Figure 1. According to these values, transformers are most likely to undergo tap-changing operations at low to medium wind injections. Transformer T_3 is the most sensitive transformer to wind injection, followed by T_4 and T_5. Furthermore, the sensitivity analysis indicates that T_3 is extremely sensitive to wind injection at WG_2.

In the next section, the continuation power flow will be used to explore key parameters of the system, with the goal of reducing the impact of wind injection at WG_2 on the tap position of transformer T_3.

III. Continuation Power Flow

Sensitivity values only provide local information around a single operating point. This can be helpful in identifying bus voltages and transformer taps that are highly sensitive to wind injection at a certain operating point. However sensitivity analysis may not accurately capture the behaviour of these variables in response to large changes in the system.

The power flow equations (1)-(2) can be written in generalized form as $f(x) = 0$, where f and x have the same dimension. This problem is fully determined, so solutions will be points. If a single parameter is allowed to vary, for example the active power at a PV or PQ bus, or the voltage setpoint at a voltage regulated bus, the problem takes the form,

$$f(x, \lambda) = 0, \tag{7}$$

where λ is the single free parameter. Now the problem has one more variable than constraint, so is under-determined. In this case, the solution is no longer a single point, but rather defines a curve. Freeing a second parameter results in a surface which can be shown as a collection of curves, i.e. contour diagram, similar to a topographic map with contours of elevation. This concept underlies the continuation power flow.

Continuation methods for solving problems of the form (7) are well documented [4], [5]. Predictor-corrector algorithms, such as the Euler homotopy method, provide a robust process for obtaining a sequence of points along the desired curve. Applications of this particular method to power system problems are discussed in [6], [7].

The continuation power flow enables a range of studies that assist in assessing the impact of wind power in weak grids, including:

1) Exploring parametric influences in the relationship between wind power injection and bus voltages, tap positions and line flows, and
2) Extending those studies to consider interactions between multiple wind-injection points.

A. Parametric effects

The continuation power flow can be used to show how certain network parameters can be adjusted to reduce the impact of wind-power variation. In the previous section we observed that at low to medium levels of wind-power injection, wind-power variability at WG_2 (in Figure 1) has a detrimental effect on the tap-changing operation of transformer T_3. We would like to determine actions that minimize the number of tap-change operations as wind injection at WG_2 varies, thereby extending transformer life. It is useful to consider the setpoint of the transformer voltage regulator, as that parameter has a significant impact on the tap position. Figure 2(a) shows a collection of contour curves, with each curve obtained by fixing the tap at a discrete value and freeing the two power-flow parameters, 1) wind injection at WG_2, and 2) voltage setpoint of T_3. Each curve corresponds to a discrete tap position, with adjacent curves corresponding to the next higher and lower taps.

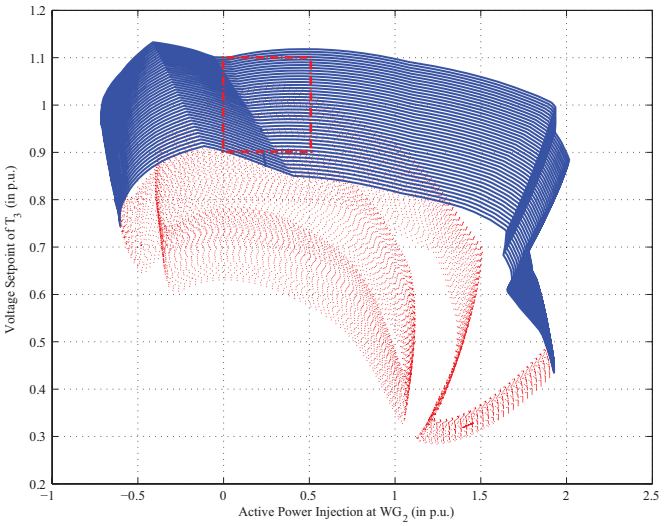

(a) Global

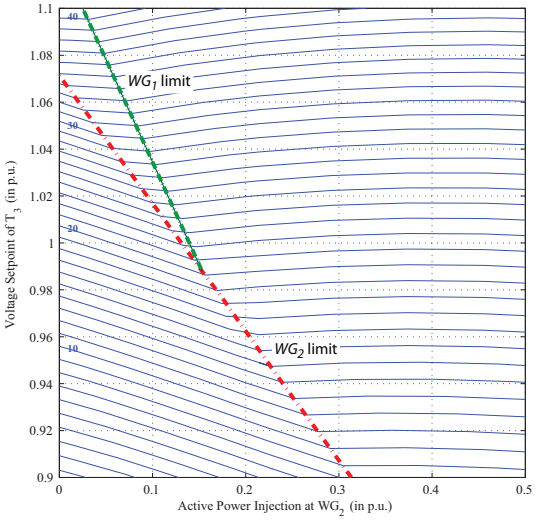

(b) Region of Interest

Fig. 2. Contour diagrams of T_3 tap position for varying active power injection at WG_2 and T_3 voltage setpoint.

Power systems incorporate numerous devices that regulate voltages, with an overall voltage profile achieved through coordination of generators, tap-changing transformers, and FACTS devices such as Statcoms and SVCs. Under normal operation these devices regulate to specified setpoints. However significant changes, such as large variations in wind-power or deviations in load, can drive these regulating devices to their limits. Regulation can no longer be achieved when a limit is encountered, so the controlled quantity will deviate from its setpoint value. The resulting change in the system description introduces discontinuities into the contours.

Two such discontinuities are apparent in Figure 2(b), where the contour lines corresponding to the inductive limits of WG_1 and WG_2 have been superimposed on the tap-position contours. As the voltage setpoint for T_3 is lowered and the WG_2 discontinuity is crossed, the slope of the tap contours

increases. As a consequence, deviations in wind injection will induce greater tap variation. It may be concluded that increasing the voltage setpoint of T_3 tends to lower the impact of WG_2 output variability on T_3 tap changing.

It should be noted that contour curves may pass through turning points where the Jacobian of the power-flow equations is singular [5]. The power-flow equations generically have multiple solutions, but usually only one solution is stable. Extraneous solutions can be easily recognized by checking the eigenvalues of the Jacobian matrix. Each time the contour curve passes through a turning point, one eigenvalue of the Jacobian changes sign. The red dotted branches in Figure 2(a) identify cases where eigenvalues have changed sign.

B. Interactions due to wind injection at multiple nodes

Wind-power injections at multiple nodes may interact to affect the behaviour of voltages and tap positions in unusual and unexpected ways. The continuation power flow provides a means of exploring such phenomena. Figure 3(a) shows the contours of voltage at load bus L_1 (highlighted in yellow in Figure 1), which is in the vicinity of wind injection nodes WG_1 and WG_2. The region of the contour diagram corresponding to the feasible range of wind-power injections is highlighted by the red box in Figure 3(a), and an enlargement of that region is provided in Figure 3(c).

Discontinuities induced by reactive power limits at the two wind-farms WG_1 and WG_2 are evident in Figure 3(a). They introduce a roughly symmetric pattern, corresponding to wind-power being high at one wind-farm and low at the other. Figure 3(b) shows the contour lines for the inductive limits of WG_1 and WG_2 superimposed on the contour diagram of Figure 3(a). As wind-power injection increases, the wind-farm must absorb more reactive power to prevent the voltage from rising. This continues until its inductive limit is encountered. As wind-power continues to increase, the voltage magnitude at the wind-farm and adjacent nodes will rise. The solution space in Figure 3(b) is divided into four regions labeled A, B, C and D. In region A, both WG_1 and WG_2 are regulating voltage. In region C, WG_2 has reached its inductive limit but WG_1 is still regulating, whereas in region D the situation is the reverse. In region B both WG_1 and WG_2 have reached their inductive limits, so no voltage regulation is possible.

IV. Quadratic Optimization for Line Congestion

In order to minimize the cost of distribution networks, distribution line designs are usually closely tied to the load profile of the network and its growth projections. The addition of substantial wind power to such networks is, therefore, likely to cause overloading of line segments.

In a meshed network with multiple points of connection to the transmission system, as in Figure 1, varying wind generation patterns may cause line flows to vary in ways that are not always obvious. Consequently, line segments that are not even necessarily near wind injection nodes may be driven to their limits as wind generation changes. On the other hand, maximum generation at all wind-farms may not cause any

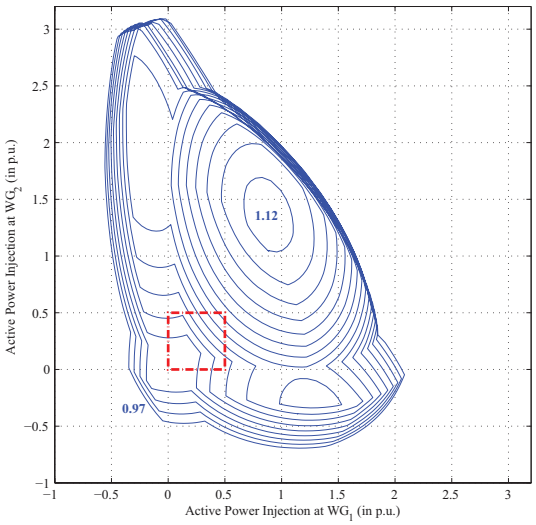

(a) Global view.

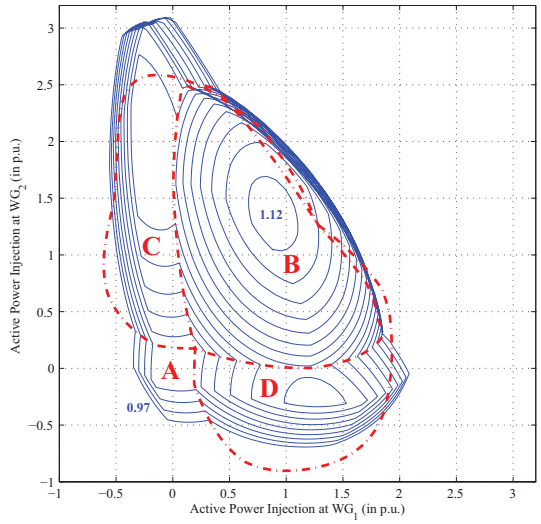

(b) Global view, including reactive limit curves.

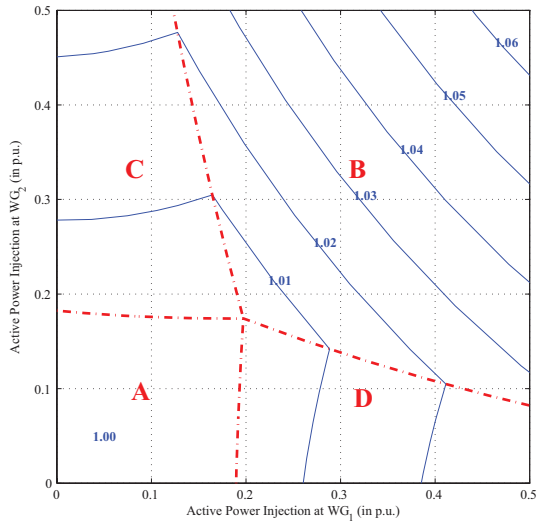

(c) Region of Interest.

Fig. 3. Contour diagrams of voltage magnitude at load bus L_1 for varying active power injections at wind nodes (± 15 MVAr compensation).

TABLE II
DC APPROXIMATION OF ACTUAL LINE FLOWS, FOR LINES HIGHLIGHTED IN GREEN IN FIGURE 1.

Line	DC Flow (%)	AC Flow (%)
1	66	55
2	45	43
3	82	84
4	107	95
5	114	90

congestion. It is therefore challenging to discover potential line overload vulnerabilities using conventional power-flow methods. To circumvent this difficulty, it would be useful to know the smallest change in the wind generation pattern that would cause any line segment to encounter its limit. This would immediately identify the most vulnerable line, as well as the most troublesome generation pattern.

Two optimization methods have been proposed for determining that information for any given operating point. Both are based on a convex quadratic optimization formulation, with the first using a DC power-flow approximation, and the second using AC sensitivities. The first of these methods shares some similarities with the instanton formulation developed in [8]. The DC method is more efficient computationally whereas the AC sensitivity-based method is more accurate. The AC approach may, however, require multiple iterations to achieve convergence, with each iteration solving a power flow and computing sensitivities. The AC formulation also does not provide any guarantee of a globally optimal solution, though our investigations have not found this to be an issue. Both methods take into account correlation between wind at different nodes.

A. DC power flow approximation

At the core of the DC quadratic optimization is the DC power flow. The usefulness of this optimization approach therefore depends on how accurately the DC power flow approximates actual line flows. It has been argued that the DC power flow may yield inaccurate approximations for networks where resistance is non-negligible ($\frac{X}{R} < 4$) [9]. However, we have found for the power system of Figure 1, where $\frac{X}{R} \approx 1$, that the DC power flow approximation is quite accurate. Table II compares the DC approximation with the accurate AC power flow for the lines highlighted in green in Figure 1. The values in the table are given as a percentage of the line rating, and correspond to the case where each of the wind-farms in Figure 1 is producing 30 MW.

B. DC quadratic optimization

Let the power generated at m wind-farms be described by the vector $\rho \in \mathbb{R}^m$. The wind-power generation pattern ρ that is closest (in a weighted 2-norm sense) to base-case generation ρ_0, and that causes line i to encounter its flow limit ℓ_i, is given by the DC quadratic optimization problem,

$$\bar{\rho}_i = \underset{\rho}{\operatorname{argmin}} \ \frac{1}{2}(\rho-\rho_0)^\top W(\rho-\rho_0) \tag{8}$$

subject to

$$\begin{bmatrix} A_\rho \\ A_b \end{bmatrix} \theta - \begin{bmatrix} \rho \\ b \end{bmatrix} = 0 \tag{9}$$

$$s_i^\top \theta - \ell_i = 0 \tag{10}$$

$$0 \le \rho \le \rho_{max} \tag{11}$$

where W is a symmetric, positive definite weighting matrix that captures the correlation between generation at the m wind-farms. For an n-bus network, bus phase angles are given by $\theta \in \mathbb{R}^{n-1}$, and non-wind power injections/loads by $b \in \mathbb{R}^{n-1-m}$. The admittance matrix $\begin{bmatrix} A_\rho \\ A_b \end{bmatrix}$ establishes a linear mapping between phase angles and power injections. Equation (10) forces the flow on a single chosen line i to equal its limit value, given by the scalar ℓ_i.

The Lagrangian [10] for this problem is given by,

$$\begin{aligned}\mathcal{L}(\rho,\theta,\lambda_\rho,\lambda_b,\gamma) =& \frac{1}{2}(\rho-\rho_0)^\top W(\rho-\rho_0) + \lambda_\rho^\top(A_\rho\theta-\rho) \\ &+ \lambda_b^\top(A_b\theta-b) + \gamma(s_i^\top\theta-\ell_i)\end{aligned} \tag{12}$$

with the Karush-Kuhn-Tucker conditions [10] yielding the set of linear equations,

$$\frac{\partial\mathcal{L}}{\partial\rho} = (\rho-\rho_0)^\top W - \lambda_\rho^\top \qquad = 0 \tag{13}$$

$$\frac{\partial\mathcal{L}}{\partial\theta} = \begin{bmatrix}\lambda_\rho^\top & \lambda_b^\top\end{bmatrix}\begin{bmatrix} A_\rho \\ A_b \end{bmatrix} + \gamma s^\top = 0 \tag{14}$$

$$\frac{\partial\mathcal{L}}{\partial\lambda_\rho} = A_\rho\theta - \rho \qquad = 0 \tag{15}$$

$$\frac{\partial\mathcal{L}}{\partial\lambda_b} = A_b\theta - b \qquad = 0 \tag{16}$$

$$\frac{\partial\mathcal{L}}{\partial\gamma} = s_i^\top\theta - \ell_i \qquad = 0 \tag{17}$$

which can be expressed in matrix form as,

$$\begin{bmatrix} W & 0 & -I & 0 & 0 \\ 0 & 0 & A_\rho^\top & A_b^\top & s_i \\ -I & A_\rho & 0 & 0 & 0 \\ 0 & A_b & 0 & 0 & 0 \\ 0 & s_i^\top & 0 & 0 & 0 \end{bmatrix}\begin{bmatrix} \rho \\ \theta \\ \lambda_\rho \\ \lambda_b \\ \gamma \end{bmatrix} = \begin{bmatrix} W\rho_0 \\ 0 \\ 0 \\ b \\ \ell_i \end{bmatrix}. \tag{18}$$

This problem can be efficiently solved for large systems using standard sparse linear solvers. Note that the base-case generation ρ_0 appears only in the right hand side of (18). Therefore a range of base-case conditions can be evaluated efficiently through forward and backward substitution.

Because (18) considers only one line limit at a time, determining the most restrictive case from a set of candidate lines requires repeated solutions, with different line parameters (s_i, ℓ_i) for each case. The modifications required in (18) for each new case are minimal though, allowing efficient partial refactorization techniques [11] to be used to reduce the computational burden. Collecting the minima for all the candidate lines into the set $P = \{\bar{\rho}_1, \bar{\rho}_2, \dots\}$, the most restrictive case is given by,

$$\rho^* = \underset{\rho\in P}{\operatorname{argmin}} \ \frac{1}{2}(\rho-\rho_0)^\top W(\rho-\rho_0). \tag{19}$$

TABLE III
MINIMAL WIND INJECTION NEEDED TO CAUSE LINE CONGESTION.

Line	WG_1	WG_2	WG_3
1	37	0	0
2	0	27	0
3	19	46	18
4	31	23	22
5	13	10	36

TABLE IV
MOST VULNERABLE LINES AT EACH OPERATING POINTS, DC OPTIMIZATION.

No.	Operating point			Congested line / $\Delta\rho$	
	WG_1	WG_2	WG_3	No Correlation	Correlation
1[a]	30	30	30	–	–
2	30	30	10	4 / [5,3,3]	4 / [4,4,4]
3	30	10	30	5 / [0,0,2]	5 / [1,1,1]
4	10	30	30	5 / [1,1,1]	5 / [1,1,1]
5	30	10	10	1 / [9 -1 -1]	1 / [10,4,4]
6	10	30	10	2 / [-3,5,-3]	2 / [-4,4,-4]
7	10	10	30	5 / [2,2,6]	5 / [4,4,5]
8	10	10	10	2 / [-10,17,-10]	5 / [14,13,19]

[a] Lines 4 and 5 are already congested according to the DC power flow approximation.

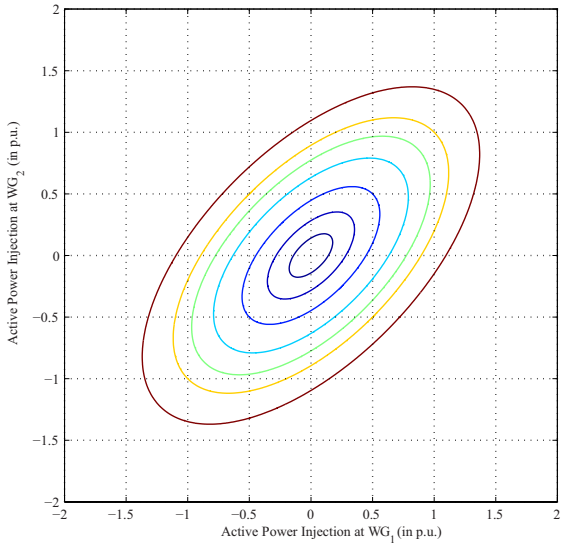

Fig. 4. Ellipsoids generated by correlation matrix (20).

The network presented in Figure 1 provides a realistic test case for illustrating the DC optimization. The three wind-farms WG_1, WG_2 and WG_3 have the potential to overload the five feeders that are labelled and highlighted in green in the network diagram. For this initial case, it was assumed the outputs of the wind-farms were not correlated, so the weighting matrix W was set to the identity matrix. Table III presents the minimal wind generation that will drive each line to its limit. These results were obtained for $\rho_0 = 0$, as we were interested in absolute generation levels rather than changes from pre-existing loading conditions.

The insights provided by the results are helpful in understanding the influence of generation on feeder loadings. Line 1, for example, reaches its maximum loading when the flow is towards the south from WG_1, in the general direction of WG_2 and WG_3. When the other wind-farms generate, they produce a counter-flow on line 1, allowing WG_1 to further increase its output. Hence line 1 in most vulnerable to overload when WG_2 and WG_3 are out of service. Similarly, line 2 reaches its limit when flow is towards the west, from WG_2 in the direction of WG_1 and WG_3. In this case, generation at WG_1 and WG_3 will produce counter-flows on line 2, so this line is most vulnerable to overloading when those generators are not producing power. In the other cases, all generators contribute to line overloading, though typically the generator that is electrically closest has the greatest influence.

The value of the DC optimization can be further illustrated by considering vulnerability of lines when the wind-farms are operating at various different output levels. Table IV lists operating points obtained from all combinations of low (10 MW) and high (30 MW) wind generation. Each case identifies the line that would reach its limit first as wind generation was increased, along with the corresponding change in wind-power production $\Delta\rho$. The effect of correlation between wind-farms was explored by first assuming no correlation, so W in (8) was simply the identity matrix. Secondly, it was assumed the three wind-farms tended to increase/decrease output in unison. In this latter case, the desired correlation matrix W was obtained by shaping the axes of the ellipsoids given by level-sets of the cost function (8). The axis in the direction $[1\ 1\ 1]^\top$ was scaled by a factor of 4 relative to the axes in the orthogonal directions. This scaling is illustrated in Figure 4, which shows a 2-dimensional projection of the level-sets. The resulting correlation matrix was

$$W = \begin{bmatrix} 3 & -1 & -1 \\ -1 & 3 & -1 \\ -1 & -1 & 3 \end{bmatrix}. \tag{20}$$

The results of Table IV again reveal interesting trends in the relationships between generation patterns and line overloads. It can be seen that whenever WG_3 is heavily loaded, line 5 is the first to become congested. This is consistent with the findings of Table III. Line 1 becomes limiting when WG_1 is heavily loaded, and the other wind-farms are not, which is again consistent with Table III. There is a similar connection between WG_2 and line 2.

The eighth case is interesting in that correlation between wind-farms clearly affects the outcome. With no correlation, the most vulnerable loading direction $\Delta\rho = [-10\ 17\ -10]^\top$ has WG_2 increasing its output, while WG_1 and WG_3 reduce theirs. This would be unlikely if the outputs of all three wind-farms tended to change in unison. With correlation taken into account, the optimization has identified the more likely scenario of $\Delta\rho = [14\ 13\ 19]^\top$, where all wind-farms undergo a similar change.

C. AC sensitivity-based quadratic optimization

The DC quadratic optimization of (19) is guaranteed to give the globally optimal solution for the approximate DC

system [10]. However, because of the approximation inherent in the DC formulation, there is no guarantee that the line limits discovered are in fact the most restrictive. The AC sensitivity-based quadratic optimization provides increased accuracy over the DC method, though at an increased computational cost, and with no guarantee of achieving global optimality.

The magnitude of the current flow over a line between two nodes i and k can be written as the function,

$$I_{ik} = I_{ik}(\theta_i, \theta_k, V_i, V_k). \tag{21}$$

Linearizing gives

$$\Delta I_{ik} = \begin{bmatrix} \frac{\partial I_{ik}}{\partial \theta_i} & \frac{\partial I_{ik}}{\partial \theta_k} & \frac{\partial I_{ik}}{\partial V_i} & \frac{\partial I_{ik}}{\partial V_k} \end{bmatrix} \begin{bmatrix} \Delta\theta_i \\ \Delta\theta_k \\ \Delta V_i \\ \Delta V_k \end{bmatrix} \tag{22}$$

where the partial derivatives are evaluated at the operating point. Also, linearizing the power flow equations, as in (3), and inverting provides an approximate linear relationship between perturbations in power injection ΔP and ΔQ, and the corresponding perturbations in the state variables $\Delta\theta$ and $\Delta\mathcal{V}$. Assuming all perturbations in power injections are zero except for $\Delta\rho$ at wind-farms, perturbations in the states associated with nodes i and k are given by,

$$\begin{bmatrix} \Delta\theta_i \\ \Delta\theta_k \\ \Delta V_i \\ \Delta V_k \end{bmatrix} = \begin{bmatrix} S_{\theta[i,\rho]} \\ S_{\theta[k,\rho]} \\ S_{V[i,\rho]} \\ S_{V[k,\rho]} \end{bmatrix} \begin{bmatrix} \Delta\rho_1 \\ \vdots \\ \Delta\rho_m \end{bmatrix} \tag{23}$$

where S_V and S_θ follow from (5) and (6) respectively, and subscript $[i,\rho]$ refers to the i-th row and the subset of columns that correspond to ρ. Combining (22) and (23) allows the change in line current ΔI_{ik} to be related directly to changes in wind generation $\Delta\rho$ through,

$$\Delta I_{ik} = S_{I\rho}\Delta\rho. \tag{24}$$

If the line current limit of I_{ik}^{lim} and operating point value I_{ik}^0 are sufficiently close, the linearization (24) can be used to establish a first-order approximation to the minimum change in wind power that would force the line to its limit. The resulting formulation is,

$$\Delta\bar{\rho}_{ik} = \underset{\Delta\rho}{\operatorname{argmin}} \ \frac{1}{2}\Delta\rho^\top W \Delta\rho \tag{25}$$

subject to

$$I_{ik}^{lim} - I_{ik}^0 = \Delta I_{ik} = S_{I\rho}\Delta\rho. \tag{26}$$

The Lagrangian for this problem can be written as,

$$\mathcal{L}(\Delta\rho, \lambda) = \frac{1}{2}\Delta\rho^\top W \Delta\rho + \lambda\big(S_{I\rho}\Delta\rho - \Delta I_{ik}\big) \tag{27}$$

with the Karush-Kuhn-Tucker conditions yielding,

$$\frac{\partial\mathcal{L}}{\partial\Delta\rho} = \Delta\rho^\top W + \lambda S_{I\rho} = 0 \tag{28}$$

$$\frac{\partial\mathcal{L}}{\partial\lambda} = S_{I\rho}\Delta\rho - \Delta I_{ik} \ = 0 \tag{29}$$

TABLE V
MOST VULNERABLE LINES AT EACH OPERATING POINTS, AC OPTIMIZATION.

No.	Operating point			Congested line / $\Delta\rho$	
	WG_1	WG_2	WG_3	No Correlation	Correlation
1	30	30	30	4 / [1,1,1]	4 / [1,1,1]
2	30	30	10	4 / [9,6,6]	4 / [8,7,7]
3	30	10	30	5 / [2,2,8]	5 / [5,5,6]
4	10	30	30	5 / [3,2,9]	5 / [5,5,7]
5	30	10	10	1 / [14,-5,-6]	4 / [14,13,13]
6	10	30	10	2 / [-8,3,-8]	3 / [12,15,12]
7	10	10	30	5 / [4,3,13]	5 / [8,8,11]
8	10	10	10	5 / [10,7,31]	4 / [22,21,20]

or more compactly,

$$\begin{bmatrix} W & S_{I\rho}^\top \\ S_{I\rho} & 0 \end{bmatrix} \begin{bmatrix} \Delta\rho \\ \lambda \end{bmatrix} = \begin{bmatrix} 0 \\ \Delta I_{ik} \end{bmatrix}. \tag{30}$$

Solving (30) is straightforward, and yields an estimate $\Delta\bar{\rho}_{ik}$ of the change in wind power output that is most likely to drive line i-k to its limit. That estimate can be used in an iterative scheme:

1) Update wind-power production $\rho + \Delta\bar{\rho}_{ik}$,
2) Solve the AC power flow for the new operating point,
3) Calculate new sensitivities, and
4) Repeat the optimization.

We have found this process converges reliably within 1-2 iterations. This iterative solution process is then repeated for each line in a specified set of candidate lines. The line that is most restrictive, in the W-norm sense of (19), establishes the most vulnerable loading direction for the wind farms.

Table V lists the lines identified as the most vulnerable for the same set of operating points as in Table IV. Again, the influence of correlation between wind-farms has been considered.

D. Comparison of the results

There is generally strong qualitative agreement between the DC and AC optimization results presented in Tables IV and V respectively. This is particularly so for the operating points that are more heavily loaded. In cases where the two methods identified different lines, the DC results were investigated further. It was found that the difference in cost (19) between the two most vulnerable lines was small. In such cases, typically the second ranked line matched the line selected by the AC optimization.

Computationally, the efficiency of the DC optimization provides a significant advantage when analyzing systems with large numbers of wind-farms and numerous lines that are susceptible to overloading.

V. CONCLUSION

The paper has presented a set of tools that are well suited to analyzing the impact of wind variability on bus voltages, voltage regulating transformers and line flows. These tools provide valuable insights into the effects of wind generation on sub-transmission and distribution networks. Because of the relative weakness of these networks, wind variability can

induce unacceptable voltage excursions, excessive transformer tapping, and line overloads. The tools that have been presented not only help identify vulnerabilities within networks, but can also offer insights into ways to retune parameters to mitigate the impacts of wind variability. This will help pave the way for higher penetration of wind and other intermittent renewable resources into weak networks.

REFERENCES

[1] S.S. Baghsorkhi and I.A. Hiskens, "Impact of wind power variability on sub-transmission networks", *Proceedings of the IEEE Power and Energy Society General Meeting*, San Diego, CA, July 2012.

[2] J.D. Glover, M.S. Sarma and T.J. Overbye, Power System Analysis and Design, 5th Edition, CL-Engineering, 2012.

[3] D.S. Bernstein, *Matrix Mathematics: Theory, Facts, and Formulas*, 2nd Edition, Princeton University Press, 2009.

[4] C.B. Garcia and W.I. Zangwill, *Pathways to Solutions, Fixed Points and Equilibria*, Prentice Hall, Englewood Cliffs, NJ, 1981.

[5] R. Seydel, *Practical Bifurcation and Stability Analysis*, 3rd Edition, Interdisciplinary Applied Mathematics, Vol. 5, Springer-Verlag, 1994.

[6] G.B. Price, "A generalized circle diagram approach for global analysis of the transmission system performance" *IEEE Transaction on Power Apparatus and Systems*, Vol. PAS-103, No. 10, October 1984, pp. 2881-2890.

[7] I.A. Hiskens and R.J. Davy, "Exploring the power flow solution space boundary", *IEEE Transactions on Power Systems*, Vol. 16, No. 3, August 2001, pp. 389-395.

[8] M. Chertkov, M. Stepanov, F. Pan, and R. Baldick, "Exact and efficient algorithm to discover extreme stochastic events in wind generation over transmission power grids", *Proceedings of the 50th IEEE Conference on Decision and Control*, Orlando, FL, December 2011, pp. 2174-2180.

[9] K. Purchala, L. Meeus, D. Van Dommeln and R. Belmans, "Usefulness of DC power flow for active power flow analysis", *Proceedings of the IEEE Power and Energy Society General Meeting*, San Francisco, CA, July 2005.

[10] J. Nocedal and S.J. Wright , *Numerical Optimization*, Springer, 2006.

[11] S.M. Chan and V. Brandwajn, "Partial matrix refactorization", *IEEE Transactions on Power Systems*, Vol. 1, No. 1, February 1986, pp. 193-199.

Sina Sadeghi Baghsorkhi (Student, IEEE) received the B.S. degree in electrical engineering from Sharif University of Technology, Tehran, Iran, in 2007 and the M.S. degree in natural resources and environment from the University of Michigan, Ann Arbor, MI, in 2009. Currently, he is working toward his Ph.D. degree in the Department of Electrical Engineering and Computer Science at the University of Michigan. His research interests are power system analysis, control and optimization, particularly as related to the integration of intermittent renewable generation. Since 2010 he has been involved in wind studies at the Detroit Edison Company (DTE) in Michigan. He is currently studying the impact of wind power on sub-transmission and distribution networks, and in particular is working on the applications of convex optimization methods to line congestion and voltage control/regulation issues arising from integration of large-scale wind power.

Ian A. Hiskens (Fellow, IEEE) received the B.Eng. degree in electrical engineering and the B.App.Sc. degree in mathematics from the Capricornia Institute of Advanced Education, Rockhampton, Australia, in 1980 and 1983 respectively, and the Ph.D. degree in electrical engineering from the University of Newcastle, Australia, in 1991.

He is the Vennema Professor of Engineering in the Department of Electrical Engineering and Computer Science, University of Michigan, Ann Arbor. He has held prior appointments in the Queensland electricity supply industry, and various universities in Australia and the United States. His major research interests lie in the area of power system analysis, in particular system dynamics and control, and security assessment. His recent activity has focused largely on integration of renewable generation and controllable load.

Dr. Hiskens is actively involved in various IEEE societies, and is VP-Finance of the IEEE Systems Council. He is a Fellow of the IEEE, a Fellow of Engineers Australia and a Chartered Professional Engineer in Australia.